PHYSICAL REVIEW D **89,** 011102(R) (2014)

Search for lepton-number violating $B^+ \to X^- \ell^+ \ell'^+$ decays

J. P. Lees,[1] V. Poireau,[1] V. Tisserand,[1] E. Grauges,[2] A. Palano,[3a,3b] G. Eigen,[4] B. Stugu,[4] D. N. Brown,[5] L. T. Kerth,[5] Yu. G. Kolomensky,[5] M. J. Lee,[5] G. Lynch,[5] H. Koch,[6] T. Schroeder,[6] C. Hearty,[7] T. S. Mattison,[7] J. A. McKenna,[7] R. Y. So,[7] A. Khan,[8] V. E. Blinov,[9a,9c] A. R. Buzykaev,[9a] V. P. Druzhinin,[9a,9b] V. B. Golubev,[9a,9b] E. A. Kravchenko,[9a,9b] A. P. Onuchin,[9a,9c] S. I. Serednyakov,[9a,9b] Yu. I. Skovpen ,[9a,9b] E. P. Solodov,[9a,9b] K. Yu. Todyshev ,[9a,9b] A. N. Yushkov,[9a] A. J. Lankford,[10] M. Mandelkern,[10] B. Dey,[11] J. W. Gary,[11] O. Long,[11] C. Campagnari,[12] M. Franco Sevilla,[12] T. M. Hong,[12] D. Kovalskyi,[12] J. D. Richman,[12] C. A. West,[12] A. M. Eisner,[13] W. S. Lockman,[13] B. A. Schumm,[13] A. Seiden,[13] D. S. Chao,[14] C. H. Cheng,[14] B. Echenard,[14] K. T. Flood,[14] D. G. Hitlin,[14] T. S. Miyashita,[14] P. Ongmongkolkul,[14] F. C. Porter,[14] R. Andreassen,[15] Z. Huard,[15] B. T. Meadows,[15] B. G. Pushpawela,[15] M. D. Sokoloff,[15] L. Sun,[15] P. C. Bloom,[16] W. T. Ford,[16] A. Gaz,[16] U. Nauenberg,[16] J. G. Smith,[16] S. R. Wagner,[16] R. Ayad,[17,*] W. H. Toki,[17] B. Spaan,[18] R. Schwierz,[19] D. Bernard,[20] M. Verderi,[20] S. Playfer,[21] D. Bettoni,[22a] C. Bozzi,[22a] R. Calabrese,[22a,22b] G. Cibinetto,[22a,22b] E. Fioravanti,[22a,22b] I. Garzia,[22a,22b] E. Luppi,[22a,22b] L. Piemontese,[22a] V. Santoro,[22a] A. Calcaterra,[23] R. de Sangro,[23] G. Finocchiaro,[23] S. Martellotti,[23] P. Patteri,[23] I. M. Peruzzi,[23,†] M. Piccolo,[23] M. Rama,[23] A. Zallo,[23] R. Contri,[24a,24b] E. Guido,[24a,24b] M. Lo Vetere ,[24a,24b] M. R. Monge,[24a,24b] S. Passaggio,[24a] C. Patrignani,[24a,24b] E. Robutti,[24a] B. Bhuyan,[25] V. Prasad,[25] M. Morii,[26] A. Adametz,[27] U. Uwer,[27] H. M. Lacker,[28] P. D. Dauncey,[29] U. Mallik,[30] C. Chen,[31] J. Cochran,[31] W. T. Meyer,[31] S. Prell,[31] H. Ahmed,[32] A. V. Gritsan,[33] N. Arnaud,[34] M. Davier,[34] D. Derkach,[34] G. Grosdidier,[34] F. Le Diberder,[34] A. M. Lutz,[34] B. Malaescu,[34,‡] P. Roudeau,[34] A. Stocchi,[34] G. Wormser,[34] D. J. Lange,[35] D. M. Wright,[35] J. P. Coleman,[36] J. R. Fry,[36] E. Gabathuler,[36] D. E. Hutchcroft,[36] D. J. Payne,[36] C. Touramanis,[36] A. J. Bevan,[37] F. Di Lodovico,[37] R. Sacco,[37] G. Cowan,[38] J. Bougher,[39] D. N. Brown,[39] C. L. Davis,[39] A. G. Denig,[40] M. Fritsch,[40] W. Gradl,[40] K. Griessinger,[40] A. Hafner,[40] E. Prencipe,[40] K. R. Schubert,[40] R. J. Barlow,[41,§] G. D. Lafferty,[41] R. Cenci,[42] B. Hamilton,[42] A. Jawahery,[42] D. A. Roberts,[42] R. Cowan,[43] D. Dujmic,[43] G. Sciolla,[43] R. Cheaib,[44] P. M. Patel,[44,¶] S. H. Robertson,[44] P. Biassoni,[45a,45b] N. Neri,[45a] F. Palombo,[45a,45b] L. Cremaldi,[46] R. Godang,[46,**] P. Sonnek,[46] D. J. Summers,[46] M. Simard,[47] P. Taras,[47] G. De Nardo ,[48a,48b] D. Monorchio,[48a,48b] G. Onorato,[48a,48b] C. Sciacca,[48a,48b] M. Martinelli,[49] G. Raven,[49] C. P. Jessop,[50] J. M. LoSecco,[50] K. Honscheid,[51] R. Kass,[51] J. Brau,[52] R. Frey,[52] N. B. Sinev,[52] D. Strom,[52] E. Torrence,[52] E. Feltresi,[53a,53b] M. Margoni,[53a,53b] M. Morandin,[53a] M. Posocco,[53a] M. Rotondo,[53a] G. Simi,[53a,53b] F. Simonetto,[53a,53b] R. Stroili,[53a,53b] S. Akar,[54] E. Ben-Haim,[54] M. Bomben,[54] G. R. Bonneaud,[54] H. Briand,[54] G. Calderini,[54] J. Chauveau,[54] Ph. Leruste,[54] G. Marchiori,[54] J. Ocariz,[54] S. Sitt,[54] M. Biasini,[55a,55b] E. Manoni,[55a] S. Pacetti,[55a,55b] A. Rossi,[55a] C. Angelini,[56a,56b] G. Batignani,[56a,56b] S. Bettarini,[56a,56b] M. Carpinelli,[56a,56b,††] G. Casarosa,[56a,56b] A. Cervelli,[56a,56b] M. Chrzaszcz,[56a,56b] F. Forti,[56a,56b] M. A. Giorgi,[56a,56b] A. Lusiani,[56a,56c] B. Oberhof,[56a,56b] E. Paoloni,[56a,56b] A. Perez,[56a] G. Rizzo,[56a,56b] J. J. Walsh,[56a] D. Lopes Pegna,[57] J. Olsen,[57] A. J. S. Smith,[57] R. Faccini,[58a,58b] F. Ferrarotto,[58a] F. Ferroni,[58a,58b] M. Gaspero,[58a,58b] L. Li Gioi ,[58a] G. Piredda,[58a] C. Bünger,[59] O. Grünberg,[59] T. Hartmann,[59] T. Leddig,[59] C. Voß,[59] R. Waldi,[59] T. Adye,[60] E. O. Olaiya,[60] F. F. Wilson,[60] S. Emery,[61] G. Hamel de Monchenault,[61] G. Vasseur,[61] Ch. Yèche,[61] F. Anulli,[62,‡‡] D. Aston,[62] D. J. Bard,[62] J. F. Benitez,[62] C. Cartaro,[62] M. R. Convery,[62] J. Dorfan,[62] G. P. Dubois-Felsmann,[62] W. Dunwoodie,[62] M. Ebert,[62] R. C. Field,[62] B. G. Fulsom,[62] A. M. Gabareen,[62] M. T. Graham,[62] C. Hast,[62] W. R. Innes,[62] P. Kim,[62] M. L. Kocian,[62] D. W. G. S. Leith,[62] P. Lewis,[62] D. Lindemann,[62] B. Lindquist,[62] S. Luitz,[62] V. Luth,[62] H. L. Lynch,[62] D. B. MacFarlane,[62] D. R. Muller,[62] H. Neal,[62] S. Nelson,[62] M. Perl,[62] T. Pulliam,[62] B. N. Ratcliff,[62] A. Roodman,[62] A. A. Salnikov,[62] R. H. Schindler,[62] A. Snyder,[62] D. Su,[62] M. K. Sullivan,[62] J. Va'vra,[62] A. P. Wagner,[62] W. F. Wang,[62] W. J. Wisniewski,[62] M. Wittgen,[62] D. H. Wright,[62] H. W. Wulsin,[62] V. Ziegler,[62] W. Park,[63] M. V. Purohit,[63] R. M. White,[63,§§] J. R. Wilson,[63] A. Randle-Conde,[64] S. J. Sekula,[64] M. Bellis,[65] P. R. Burchat,[65] E. M. T. Puccio,[65] M. S. Alam,[66] J. A. Ernst,[66] R. Gorodeisky,[67] N. Guttman,[67] D. R. Peimer,[67] A. Soffer,[67] S. M. Spanier,[68] J. L. Ritchie,[69] A. M. Ruland,[69] R. F. Schwitters,[69] B. C. Wray,[69] J. M. Izen,[70] X. C. Lou,[70] F. Bianchi,[71a,71b] F. De Mori,[71a,71b] A. Filippi,[71a] D. Gamba,[71a,71b] S. Zambito,[71a,71b] L. Lanceri,[72a,72b] L. Vitale,[72a,72b] F. Martinez-Vidal,[73] A. Oyanguren,[73] P. Villanueva-Perez,[73] J. Albert,[74] Sw. Banerjee,[74] F. U. Bernlochner,[74] H. H. F. Choi,[74] G. J. King,[74] R. Kowalewski,[74] M. J. Lewczuk,[74] T. Lueck,[74] I. M. Nugent,[74] J. M. Roney,[74] R. J. Sobie,[74] N. Tasneem,[74] T. J. Gershon,[75] P. F. Harrison,[75] T. E. Latham,[75] H. R. Band,[76] S. Dasu,[76] Y. Pan,[76] R. Prepost,[76] S. L. Wu[76]

(*BABAR* Collaboration)

[1]*Laboratoire d'Annecy-le-Vieux de Physique des Particules (LAPP), Université de Savoie, CNRS/IN2P3, F-74941 Annecy-Le-Vieux, France*
[2]*Universitat de Barcelona, Facultat de Fisica, Departament ECM, E-08028 Barcelona, Spain*
[3a]*INFN Sezione di Bari, I-70126 Bari, Italy*
[3b]*Dipartimento di Fisica, Università di Bari, I-70126 Bari, Italy*
[4]*University of Bergen, Institute of Physics, N-5007 Bergen, Norway*
[5]*Lawrence Berkeley National Laboratory and University of California, Berkeley, California 94720, USA*

[6]*Ruhr Universität Bochum, Institut für Experimentalphysik 1, D-44780 Bochum, Germany*
[7]*University of British Columbia, Vancouver, British Columbia, Canada V6T 1Z1*
[8]*Brunel University, Uxbridge, Middlesex UB8 3PH, United Kingdom*
[9a]*Budker Institute of Nuclear Physics SB RAS, Novosibirsk 630090, Russia*
[9b]*Novosibirsk State University, Novosibirsk 630090, Russia*
[9c]*Novosibirsk State Technical University, Novosibirsk 630092, Russia*
[10]*University of California at Irvine, Irvine, California 92697, USA*
[11]*University of California at Riverside, Riverside, California 92521, USA*
[12]*University of California at Santa Barbara, Santa Barbara, California 93106, USA*
[13]*University of California at Santa Cruz, Institute for Particle Physics, Santa Cruz, California 95064, USA*
[14]*California Institute of Technology, Pasadena, California 91125, USA*
[15]*University of Cincinnati, Cincinnati, Ohio 45221, USA*
[16]*University of Colorado, Boulder, Colorado 80309, USA*
[17]*Colorado State University, Fort Collins, Colorado 80523, USA*
[18]*Technische Universität Dortmund, Fakultät Physik, D-44221 Dortmund, Germany*
[19]*Technische Universität Dresden, Institut für Kern- und Teilchenphysik, D-01062 Dresden, Germany*
[20]*Laboratoire Leprince-Ringuet, Ecole Polytechnique, CNRS/IN2P3, F-91128 Palaiseau, France*
[21]*University of Edinburgh, Edinburgh EH9 3JZ, United Kingdom*
[22a]*INFN Sezione di Ferrara, I-44122 Ferrara, Italy*
[22b]*Dipartimento di Fisica e Scienze della Terra, Università di Ferrara, I-44122 Ferrara, Italy*
[23]*INFN Laboratori Nazionali di Frascati, I-00044 Frascati, Italy*
[24a]*INFN Sezione di Genova, I-16146 Genova, Italy*
[24b]*Dipartimento di Fisica, Università di Genova, I-16146 Genova, Italy*
[25]*Indian Institute of Technology Guwahati, Guwahati, Assam 781 039, India*
[26]*Harvard University, Cambridge, Massachusetts 02138, USA*
[27]*Universität Heidelberg, Physikalisches Institut, D-69120 Heidelberg, Germany*
[28]*Humboldt-Universität zu Berlin, Institut für Physik, D-12489 Berlin, Germany*
[29]*Imperial College London, London SW7 2AZ, United Kingdom*
[30]*University of Iowa, Iowa City, Iowa 52242, USA*
[31]*Iowa State University, Ames, Iowa 50011-3160, USA*
[32]*Physics Department, Jazan University, Jazan 22822, Kingdom of Saudia Arabia*
[33]*Johns Hopkins University, Baltimore, Maryland 21218, USA*
[34]*Laboratoire de l'Accélérateur Linéaire, IN2P3/CNRS et Université Paris-Sud 11, Centre Scientifique d'Orsay, F-91898 Orsay Cedex, France*
[35]*Lawrence Livermore National Laboratory, Livermore, California 94550, USA*
[36]*University of Liverpool, Liverpool L69 7ZE, United Kingdom*
[37]*Queen Mary, University of London, London, E1 4NS, United Kingdom*
[38]*University of London, Royal Holloway and Bedford New College, Egham, Surrey TW20 0EX, United Kingdom*
[39]*University of Louisville, Louisville, Kentucky 40292, USA*
[40]*Johannes Gutenberg-Universität Mainz, Institut für Kernphysik, D-55099 Mainz, Germany*
[41]*University of Manchester, Manchester M13 9PL, United Kingdom*
[42]*University of Maryland, College Park, Maryland 20742, USA*
[43]*Massachusetts Institute of Technology, Laboratory for Nuclear Science, Cambridge, Massachusetts 02139, USA*
[44]*McGill University, Montréal, Québec, Canada H3A 2T8*
[45a]*INFN Sezione di Milano, I-20133 Milano, Italy*
[45b]*Dipartimento di Fisica, Università di Milano, I-20133 Milano, Italy*
[46]*University of Mississippi, University, Mississippi 38677, USA*
[47]*Université de Montréal, Physique des Particules, Montréal, Québec, Canada H3C 3J7*
[48a]*INFN Sezione di Napoli, I-80126 Napoli, Italy*
[48b]*Dipartimento di Scienze Fisiche, Università di Napoli Federico II, I-80126 Napoli, Italy*
[49]*NIKHEF, National Institute for Nuclear Physics and High Energy Physics, NL-1009 DB Amsterdam, The Netherlands*
[50]*University of Notre Dame, Notre Dame, Indiana 46556, USA*
[51]*Ohio State University, Columbus, Ohio 43210, USA*
[52]*University of Oregon, Eugene, Oregon 97403, USA*
[53a]*INFN Sezione di Padova, I-35131 Padova, Italy*
[53b]*Dipartimento di Fisica, Università di Padova, I-35131 Padova, Italy*

[54]Laboratoire de Physique Nucléaire et de Hautes Energies, IN2P3/CNRS, Université Pierre et Marie Curie-Paris6, Université Denis Diderot-Paris7, F-75252 Paris, France
[55a]INFN Sezione di Perugia, I-06123 Perugia, Italy
[55b]Dipartimento di Fisica, Università di Perugia, I-06123 Perugia, Italy
[56a]INFN Sezione di Pisa, I-56127 Pisa, Italy
[56b]Dipartimento di Fisica, Università di Pisa, I-56127 Pisa, Italy
[56c]Scuola Normale Superiore di Pisa, I-56127 Pisa, Italy
[57]Princeton University, Princeton, New Jersey 08544, USA
[58a]INFN Sezione di Roma, I-00185 Roma, Italy
[58b]Dipartimento di Fisica, Università di Roma La Sapienza, I-00185 Roma, Italy
[59]Universität Rostock, D-18051 Rostock, Germany
[60]Rutherford Appleton Laboratory, Chilton, Didcot, Oxon OX11 0QX, United Kingdom
[61]CEA, Irfu, SPP, Centre de Saclay, F-91191 Gif-sur-Yvette, France
[62]SLAC National Accelerator Laboratory, Stanford, California 94309 USA
[63]University of South Carolina, Columbia, South Carolina 29208, USA
[64]Southern Methodist University, Dallas, Texas 75275, USA
[65]Stanford University, Stanford, California 94305-4060, USA
[66]State University of New York, Albany, New York 12222, USA
[67]Tel Aviv University, School of Physics and Astronomy, Tel Aviv, 69978, Israel
[68]University of Tennessee, Knoxville, Tennessee 37996, USA
[69]University of Texas at Austin, Austin, Texas 78712, USA
[70]University of Texas at Dallas, Richardson, Texas 75083, USA
[71a]INFN Sezione di Torino, I-10125 Torino, Italy
[71b]Dipartimento di Fisica, Università di Torino, I-10125 Torino, Italy
[72a]INFN Sezione di Trieste, I-34127 Trieste, Italy
[72b]Dipartimento di Fisica, Università di Trieste, I-34127 Trieste, Italy
[73]IFIC, Universitat de Valencia-CSIC, E-46071 Valencia, Spain
[74]University of Victoria, Victoria, British Columbia, Canada V8W 3P6
[75]Department of Physics, University of Warwick, Coventry CV4 7AL, United Kingdom
[76]University of Wisconsin, Madison, Wisconsin 53706, USA
(Received 5 November 2013; published 28 January 2014)

We report on a search for eleven lepton-number violating processes $B^+ \to X^- \ell^+ \ell'^+$ with $X^- = K^-, \pi^-, \rho^-, K^{*-}$, or D^- and $\ell^+/\ell'^+ = e^+$ or μ^+, using a sample of 471 ± 3 million $B\bar{B}$ events collected with the *BABAR* detector at the PEP-II e^+e^- collider at the SLAC National Accelerator Laboratory. We find no evidence for any of these modes and place 90% confidence level upper limits on their branching fractions in the range $(1.5\text{–}26) \times 10^{-7}$.

DOI: 10.1103/PhysRevD.89.011102 PACS numbers: 13.20.He, 14.60.St, 11.30.Fs

In the Standard Model (SM), lepton-number conservation holds in low-energy collisions and decays, but it can be violated in high-energy or high-density interactions [1]. The observation of neutrino oscillations [2] indicates that neutrinos have mass and, if the neutrinos are of the Majorana type, the neutrino and antineutrino are the same particle and processes that involve lepton-number violation become possible [3]. Many models beyond the SM predict that the lepton number is violated, possibly at rates approaching those accessible with current data [4]. Lepton-number violation is also a necessary condition for leptogenesis as an explanation of the baryon asymmetry of the Universe [5].

Following recent results from LHCb [6], *BABAR* [7], and Belle [8], there has been interest in the possibility of measuring the lepton-number violating (LNV) processes $B^+ \to X^- \ell^+ \ell'^+$, where X^- is a charged hadronic particle or resonance, and $\ell^+/\ell'^+ = e^+$ or μ^+ [9]. Earlier searches for these decays by the CLEO collaboration produced 90% C.L. upper limits on the branching fractions in the range $(1.0\text{–}8.3) \times 10^{-6}$ [10]. The LHCb collaboration reported 95% C.L. upper limits on the branching fractions $\mathcal{B}(B^+ \to K^- \mu^+ \mu^+) < 5.4 \times 10^{-8}$ and

*Now at the University of Tabuk, Tabuk 71491, Saudi Arabia
†Also with Università di Perugia, Dipartimento di Fisica, Perugia, Italy
‡Now at Laboratoire de Physique Nucléaire et de Hautes Energies, IN2P3/CNRS, Paris, France
§Now at the University of Huddersfield, Huddersfield HD1 3DH, UK
¶Deceased
**Now at University of South Alabama, Mobile, Alabama 36688, USA
††Also with Università di Sassari, Sassari, Italy
‡‡Also with INFN Sezione di Roma, Roma, Italy
§§Now at Universidad Técnica Federico Santa Maria, Valparaiso, Chile 2390123

$\mathcal{B}(B^+ \to \pi^- \mu^+ \mu^+) < 1.3 \times 10^{-8}$ [6]. The Belle collaboration placed 90% C.L. upper limits on the branching fractions $\mathcal{B}(B^+ \to D^- \ell^+ \ell'^+)$ in the range $(1.1\text{–}2.6) \times 10^{-6}$ [8].

We report here on a search for $B^+ \to X^- \ell^+ \ell'^+$ with $X^- = K^-, \pi^-, \rho^-, K^{*-}$, or D^- and $\ell^+/\ell'^+ = e^+$ or μ^+. We exclude the four combinations previously measured by the *BABAR* collaboration [7]. We use a data sample of 471 ± 3 million $B\bar{B}$ pairs, equivalent to an integrated luminosity of 429 fb^{-1} [11], collected at the $\Upsilon(4S)$ resonance with the *BABAR* detector at the PEP-II asymmetric-energy e^+e^- collider at the SLAC National Accelerator Laboratory. The e^+e^- c.m. energy is $\sqrt{s} = 10.58$ GeV, corresponding to the mass of the $\Upsilon(4S)$ resonance (on-resonance data). The *BABAR* detector is described in detail in Ref. [12].

Monte Carlo (MC) simulation is used to identify the background contamination, calculate selection efficiencies, evaluate systematic uncertainties, and cross-check the selection procedure. The signal channels are simulated by the EvtGen [13] package using a three-body phase space model. We also generate light quark $q\bar{q}$ continuum events ($e^+e^- \to q\bar{q}$, $q = u, d, s$), charm $e^+e^- \to c\bar{c}$ continuum events, $e^+e^- \to \mu^+\mu^-(\gamma)$, Bhabha elastic e^+e^- scattering, $B\bar{B}$ background, and two-photon events [14]. Final-state radiation is provided by Photos [15]. The detector response is simulated with GEANT4 [16], and all simulated events are reconstructed in the same manner as the data.

Particle identification is applied to all charged tracks. The charged pions and kaons are identified by measurements of their energy loss in the tracking detectors, and the number of photons and the Cherenkov angle recorded by the ring-imaging Cherenkov detector. These measurements are combined with information from the electromagnetic calorimeter and the muon detector to identify electrons and muons [12].

We select events that have four or more charged tracks, at least two of which must be identified as leptons. The ratio of the second-to-zeroth Fox–Wolfram moments [17] of the event must be less than 0.5, and the two charged leptons must have the same sign and momenta greater than 0.3 GeV/c in the laboratory frame. The separation along the beam axis between the two leptons at their closest approach to the beam line is required to be less than 0.2 cm . The combined momentum of the $\ell^+\ell'^+$ pair in the c.m. system must be less than 2.5 GeV/c. Electrons and positrons from photon conversions are removed, where photon conversion is indicated by electron-positron pairs with an invariant mass less than 0.03 GeV/c^2 and a production vertex more than 2 cm from the beam axis.

The K^{*-} is reconstructed through its decay to $K^0_S\pi^-$ and $K^-\pi^0$; the ρ^- and D^- are reconstructed through their decays to $\pi^-\pi^0$ and $K^+\pi^-\pi^-$, respectively. The photons from the π^0 must have an energy greater than 0.03 GeV, and the π^0 is required to have an energy greater than 0.2 GeV , both measured in the laboratory frame. The reconstructed π^0 invariant mass must be between 0.12 and 0.16 GeV/c^2. The invariant mass of the ρ^- is required to be between 0.470 and 1.07 GeV/c^2. The K^0_S must have an opening angle θ between its flight direction (defined as the vector between the B meson and K^0_S vertices) and its momentum vector such that $\cos\theta > 0.999$, a transverse flight distance greater than 0.2 cm, a lifetime significance $\tau/\sigma_\tau > 10$, and a reconstructed invariant mass between 0.488 and 0.508 GeV/c^2. We require the D^- invariant mass to be between 1.835 and 1.895 GeV/c^2. The invariant mass ranges are chosen to be wide enough to allow the background event distributions to be modeled.

The two leptons are combined with either a resonance candidate or a charged track to form a B-meson candidate. For muon modes, the invariant mass of each combination of a muon and a charged track from the B-meson candidate must be outside the region $3.05 < m_{\ell^+h^-} < 3.13$ GeV/c^2. This rejects events where a muon from a J/ψ decay is misidentified as a pion. The probability to misidentify a pion as a muon is approximately 2% and to misidentify as an electron is less than 0.1%.

We measure the kinematic variables $m_{\rm ES} = \sqrt{(s/2 + \mathbf{p}_0 \cdot \mathbf{p}_B)^2/E_0^2 - \mathbf{p}_B^2}$ and $\Delta E = E_B^* - \sqrt{s}/2$, where $(E_0, \mathbf{p}_0)$ is the 4-momentum of the c.m. system and $\mathbf{p}_B$ is the B candidate momentum vector, both measured in the laboratory frame; $\sqrt{s}$ is the total c.m. energy; and E_B^* is the energy of the B candidate in the c.m. system. For signal events, the $m_{\rm ES}$ distribution peaks at the B meson mass with a resolution of about 2.5 MeV/c^2, and the ΔE distribution peaks near zero with a resolution of about 20 MeV. The B candidate is required to be in the kinematic region $5.240 < m_{\rm ES} < 5.289$ GeV/c^2. The ΔE range depends on the mode but always satisfies $|\Delta E| < 0.3$ GeV.

The backgrounds arising from $q\bar{q}$, $c\bar{c}$, and $B\bar{B}$ events are suppressed through the use of a boosted decision tree discriminant (BDT) [18]. The BDT has nine inputs: the ratio of the second- and zeroth-order Fox–Wolfram moments based on the magnitude of the momentum of all neutral clusters and charged tracks in the rest of the event (ROE) not associated with the B candidate; the absolute value of the cosine of the angle between the B momentum and the beam axis in the c.m. frame; the absolute value of the cosine of the angle between the B thrust axis [19] and the beam axis in the c.m. frame; the absolute value of the cosine of the angle between the B thrust axis and the thrust axis of the ROE in the c.m. frame; the output of the flavor tagging algorithm [20]; the separation along the beam axis between the two leptons at their points of closest approach to the beam line; the missing energy in the c.m.; the momentum of the lepton pair in the c.m.; and the boost-corrected proper-time difference between the decays of the two B mesons divided by its variance. The second B meson is formed by creating a vertex from the remaining tracks that are consistent with originating from the interaction region. The discriminant is trained for each signal mode using on-resonance data with

$m_{\rm ES} < 5.27\ {\rm GeV}/c^2$ together with samples of simulated signal and background events. We compare the distributions of the data and the simulated background variables used as input to the BDTs and confirm that they are consistent.

After the application of all selection criteria, some events will contain more than one reconstructed B candidate. From the simulation sample, we estimate that the fraction of signal events with a π^0 that have more than one candidate is 30%, 13% for signal events with a K^0_S, and less than 6% for signal events where the lepton pair is combined with a D^-, K^-, or π^0. We select the most probable B candidate from among all the candidates in the event using the χ^2 from the B candidate vertex fit. Averaged over all simulated signal events, the correct B candidate is selected with an accuracy of more than 83% for the signal events with a π^0, greater than 96% for signal events with a K^0_S, and over 99% for signal events where the lepton pair is combined with a D^-, K^-, or π^-. The final event selection efficiency for simulated signal is between 6% and 16%, depending on the final state. Figure 1 shows the variation of the selection efficiency as a function of the reconstructed invariant mass $m_{X^-\ell^+}$, calculated for both leptons, for four of the modes. The remaining modes have similar distributions.

For each mode, we extract the signal and background yields from the data with an unbinned maximum likelihood (ML) fit [21] using

$$\mathcal{L} = \frac{1}{N!}\ \exp\left(-\sum_j n_j\right)\prod_{i=1}^{N}\left[\sum_j n_j \mathcal{P}_j(\vec{x}_i;\vec{\alpha}_j)\right], \qquad (1)$$

where the likelihood for each event candidate i is the sum of $n_j\mathcal{P}_j(\vec{x}_i;\vec{\alpha}_j)$ over two categories j: the signal mode $B^+ \to X^-\ell^+\ell'^+$ (including the small number of misreconstructed signal candidates) and background, as will be discussed. For each category j, $\mathcal{P}_j(\vec{x}_i;\vec{\alpha}_j)$ is the product of the probability density functions (PDFs) evaluated for the ith event's measured variables $\vec{x}_i$. The number of events for category j is denoted by n_j, and N is the total number of events in the sample. The quantities $\vec{\alpha}_j$ represent the parameters, such as means and widths, that describe the shape of the expected distributions of the measured variables for each category j. Each discriminating variable $\vec{x}_i$ in the likelihood function is modeled with a PDF, where the parameters $\vec{\alpha}_j$ are extracted from MC simulation or on-resonance data with $m_{\rm ES} < 5.27\ {\rm GeV}/c^2$. The variables $\vec{x}_i$ used in the fit are $m_{\rm ES}$, ΔE, and the multivariate discriminant BDT output; for modes involving a resonance, the resonance invariant mass is included as a fourth variable. The linear correlations between the four variables are found to be typically 4%–9% for simulated signal modes. Only $B^+ \to D^- e^+ e^+$ shows a larger correlation, between the invariant mass and ΔE, due to the occasional bremsstrahlung energy loss from the electrons. We take each $\mathcal{P}_j$ to be the product of the PDFs for the separate variables and treat any correlations in the variables later as a source of systematic uncertainty.

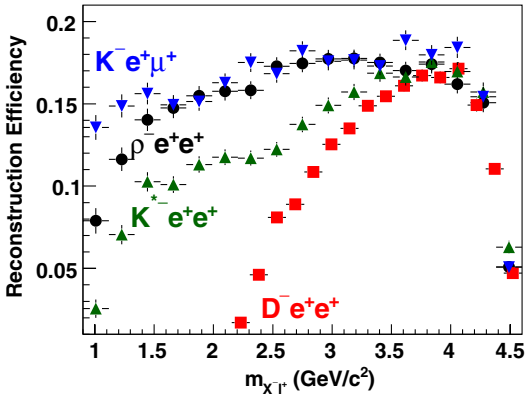

FIG. 1 (color online). Reconstruction efficiency as a function of $m_{X^-\ell^+}$ for four of the modes: $B^+ \to K^- e^+ \mu^+$ (down triangle), $B^+ \to \rho^- e^+ e^+$ (circle), $B^+ \to K^{*-}(\to K^0_S\pi^-)e^+e^+$ (up triangle), and $B^+ \to D^- e^+ e^+$ (square).

MC simulations show that the $q\bar{q}$, $c\bar{c}$, and $B\bar{B}$ backgrounds have similar distributions in the four variables after the selection criteria have been applied, and we therefore use a single background parameterization. An ARGUS parametrization [22] is used to describe the $m_{\rm ES}$ distribution. For ΔE, a first- or second-order polynomial is used or, for modes with a D meson, a Cruijff function [23]. The multivariate discriminant BDT output is fitted using a nonparametric kernel estimation KEYS algorithm [24]. The mass distributions for modes with a resonance are fitted with a first-order polynomial, together with a Gaussian function if the resonance is present in the backgrounds.

For the signal, the $m_{\rm ES}$ distribution is parametrized with a Crystal Ball function [25]. A Crystal Ball function is also used for ΔE , together with a first-order polynomial for modes with a π^0. The multivariate discriminant BDT output is taken directly from the MC distribution using a histogram. For the resonances, the signal masses are parametrized with two Gaussians, a relativistic Breit–Wigner function, and a Gounaris–Sakurai function [26] for the D^-, K^{*-}, and ρ^-, respectively. The free parameters in the ML fit are the signal and background event yields, the slope of the background $m_{\rm ES}$ distribution, and the polynomial parameters of the background ΔE and mass distributions.

We test the performance of the fits to $B^+ \to X^-\ell^+\ell'^+$ by generating ensembles of MC data sets from both the PDF distributions and the fully simulated MC events; in the latter case, the correlations between the variables are correctly simulated. We generate and fit 10,000 data sets with the numbers of signal and background events allowed to fluctuate according to a Poisson distribution. The signal yield bias in the ensemble of fits is between −0.3 and 1.2 events, depending on the mode, and this is subtracted from the yield obtained from the data.

As a cross-check of the background PDFs, we perform a fit to a simulated background sample, with the same number of events as the on-resonance data sample. The number of fitted signal events is compatible with zero for all modes. We also perform a blinded fit to the on-resonance data for each mode and confirm that the distributions of the background events are reproduced by the background PDFs. Events are identified as background if $\mathcal{P}_{\rm bck}/(\mathcal{P}_{\rm bck}+\mathcal{P}_{\rm sig})>0.9$, where $\mathcal{P}_{\rm sig}$ and $\mathcal{P}_{\rm bck}$ are computed for each event for the signal and background, respectively, without the use of the variable under consideration [27].

BABAR has previously published, using a different selection technique, four measurements of LNV in $B^+\to h^-\ell^+\ell^+$, where $h^-=K^-$ or π^-, and $\ell^+\ell^+=e^+e^+$ or $\mu^+\mu^+$ [7]. To validate the analysis reported here and as a cross-check only, we repeat the previous measurements, using the selection criteria described in this article. The reconstruction efficiencies are lower using this current analysis, and the measured 90% C.L. branching fraction upper limits are less stringent compared to the previous results by between 3% and 80%, depending on the mode. This is compatible with the use here of a generic selection procedure for the eleven reported modes.

The results of the ML fits to the on-resonance data are summarized in Table I. The signal significance is defined as $\mathcal{S}=\sqrt{2\Delta\ \ln\mathcal{L}}$, where $\Delta\ \ln\mathcal{L}$ is the change in log likelihood from the maximum value to the value when the number of signal events is set to zero. Systematic errors are included in the $\ln\mathcal{L}$ distribution by convolving the likelihood function with a Gaussian distribution with a standard deviation equal to the total systematic uncertainty, defined later in this article. If the log likelihood corresponds to a negative signal, we assign a significance of zero. The branching fraction $\mathcal{B}$ is given by $n_{\rm s}/(\eta N_{B\bar{B}})$, where $n_{\rm s}$ is the signal yield, corrected for the fit bias, η is the reconstruction efficiency, and $N_{B\bar{B}}$ is the number of $B\bar{B}$ pairs collected. We assume equal production rates of B^+B^- and $B^0\bar{B}^0$ mesons.

Figures 2 and 3 show the projections of the fit onto the discriminating variables for two of the modes, $B^+\to\pi^-e^+\mu^+$ and $B^+\to K^{*-}\mu^+\mu^+$ ($K^{*-}\to K^0_S\pi^-$). The candidates in the figure are subject to the requirement on the probability ratio $\mathcal{P}_{\rm sig}/(\mathcal{P}_{\rm bck}+\mathcal{P}_{\rm sig})>0.9$, where $\mathcal{P}_{\rm sig}$ and $\mathcal{P}_{\rm bck}$ are computed without the use of the variable plotted. The other modes show similar distributions.

The systematic uncertainties in the branching fractions arise from the PDF parametrization, fit biases, background yields, and efficiencies. The PDF uncertainties are calculated by varying, within their errors, the PDF parameters that are held fixed in the default fit, taking into account correlations. For the KEYS algorithm, we vary the smearing parameter between 50% and 150% of the nominal value [24], and for the histograms we change the number of bins used. The uncertainty for the fit bias includes the statistical uncertainty in the mean difference between the fitted signal yield from the ensemble of 10,000 MC data sets described above and the signal yield from the fit to the default MC sample, and half of the correction itself, added in quadrature.

To calculate the contribution to the uncertainty caused by the assumption that the $q\bar{q}$, $c\bar{c}$, and $B\bar{B}$ backgrounds have similar distributions, we first vary the relative proportions of $q\bar{q}$, $c\bar{c}$, and $B\bar{B}$ used in the simulated background between 0% and 100% and retrain the BDT function for each variation. The new simulated background BDT PDF is then used in the fit to the data, and the fitted yields

TABLE I. Summary of results for the measured B decay modes: total number of events in analysis region, signal yield $n_{\rm s}$ (corrected for fit bias) and its statistical uncertainty, reconstruction efficiency η, daughter branching fraction product $\Pi\mathcal{B}_i(\%)$, significance S (systematic uncertainties included), measured branching fraction $\mathcal{B}$, and the 90% C.L. upper limit ($\mathcal{B}_{UL}$).

Mode	Events	Yield	$\eta(\%)$	$\Pi\mathcal{B}_i(\%)$	S(σ)	$\mathcal{B}\,(\times10^{-7})$	$\mathcal{B}_{UL}\,(\times10^{-7})$
$B^+\to K^{*-}e^+e^+$					1.2	$1.7\pm1.4\pm0.1$	4.0
$K^{*-}\to K^-\pi^0$	63	3.8 ± 3.3	11.5 ± 0.1	33.3	1.2	$2.1\pm1.8\pm0.2$	5.1
$K^{*-}\to K^0_S\pi^-$	91	0.8 ± 3.9	12.3 ± 0.1	22.8	0.3	$0.6\pm2.9\pm0.2$	6.0
$B^+\to K^{*-}e^+\mu^+$					0.0	$-4.5\pm2.6\pm0.4$	3.0
$K^{*-}\to K^-\pi^0$	117	-1.9 ± 4.7	7.9 ± 0.1	33.3	0.0	$-1.5\pm3.8\pm0.4$	6.5
$K^{*-}\to K^0_S\pi^-$	172	-5.1 ± 2.6	8.5 ± 0.1	22.8	0.0	$-6.0\pm2.8\pm0.7$	4.2
$B^+\to K^{*-}\mu^+\mu^+$					1.3	$2.4\pm1.8\pm0.4$	5.9
$K^{*-}\to K^-\pi^0$	85	2.3 ± 1.8	6.1 ± 0.1	33.3	1.3	$2.0\pm1.8\pm0.2$	7.0
$K^{*-}\to K^0_S\pi^-$	98	2.0 ± 1.8	5.8 ± 0.1	22.8	1.0	$3.1\pm2.9\pm0.9$	9.8
$B^+\to\rho^-e^+e^+$	411	-2.1 ± 5.7	12.1 ± 0.1	100.0	0.0	$-0.4\pm1.0\pm0.1$	1.7
$B^+\to\rho^-e^+\mu^+$	1651	4.6 ± 11.4	10.3 ± 0.1	100.0	0.4	$1.0\pm2.4\pm0.2$	4.7
$B^+\to\rho^-\mu^+\mu^+$	936	2.9 ± 6.8	7.3 ± 0.1	100.0	0.5	$0.9\pm2.0\pm0.3$	4.2
$B^+\to D^-e^+e^+$	401	3.9 ± 4.8	10.2 ± 0.1	9.13	1.0	$8.8\pm8.6\pm1.5$	26
$B^+\to D^-e^+\mu^+$	549	1.1 ± 3.2	7.7 ± 0.1	9.13	0.5	$3.4\pm9.4\pm1.1$	21
$B^+\to D^-\mu^+\mu^+$	229	-1.7 ± 2.5	5.7 ± 0.1	9.13	0.0	$-6.5\pm9.9\pm0.9$	17
$B^+\to K^-e^+\mu^+$	117	5.5 ± 3.5	15.2 ± 0.1	100.0	1.8	$0.6\pm0.5\pm0.1$	1.6
$B^+\to\pi^-e^+\mu^+$	464	3.8 ± 3.5	16.4 ± 0.2	100.0	1.2	$0.5\pm0.5\pm0.1$	1.5

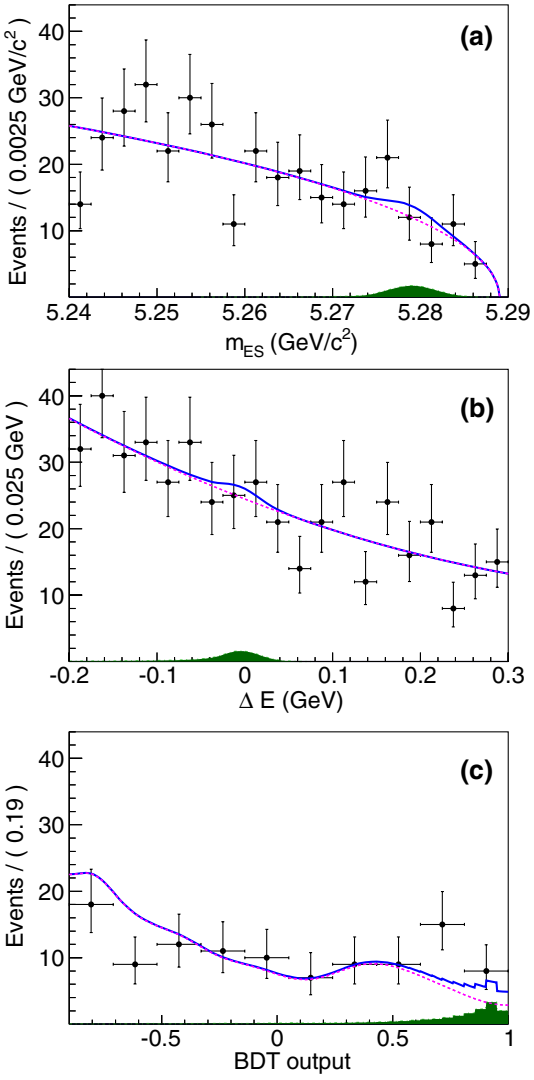

FIG. 2 (color online). Projections of the multidimensional fit onto a) $m_{\rm ES}$, b) ΔE, and c) BDT output for the mode $B^+ \to \pi^- e^+ \mu^+$. The points with error bars show the data, the dashed line is the background PDF, the solid line is the signal-plus-background PDF, and the solid area is the signal PDF.

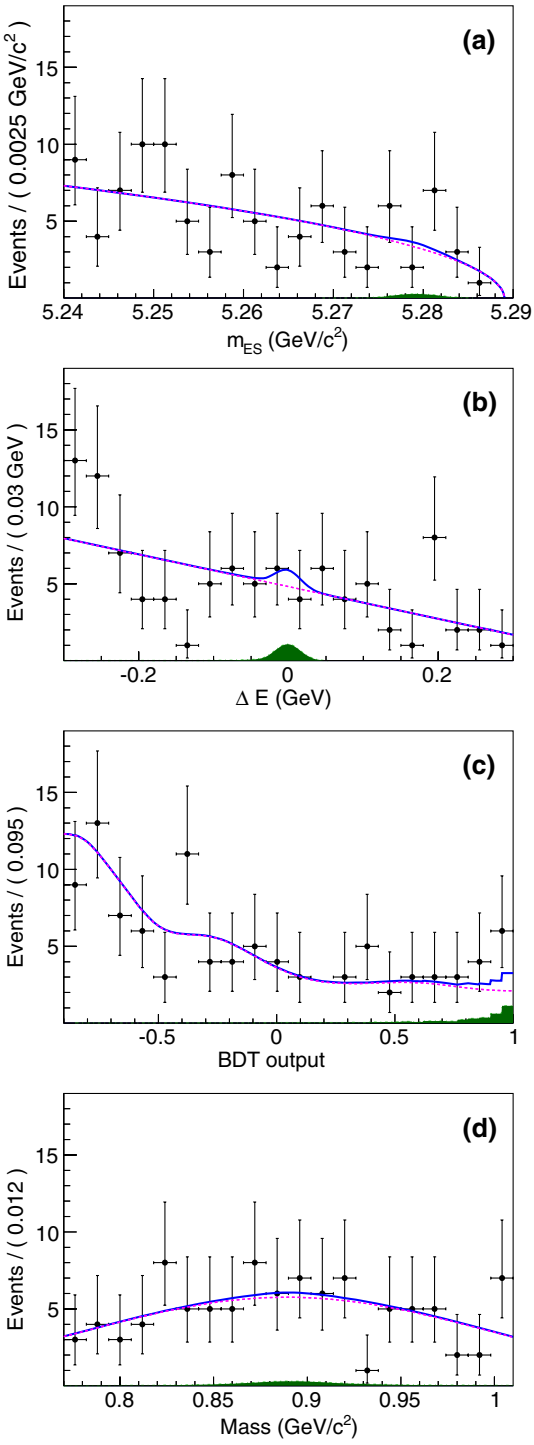

FIG. 3 (color online). Projections of the multidimensional fit onto a) $m_{\rm ES}$, b) ΔE, c) BDT output, and d) mass for the mode $B^+ \to K^{*-}\mu^+\mu^+$ ($K^{*-} \to K^0_S\pi^-$). The points with error bars show the data, the dashed line is the background PDF, the solid line is the signal-plus-background PDF, and the solid area is the signal PDF.

compared to the default fit to the data. The uncertainty is taken to be half the difference between the default fit and the maximum deviation seen in the ensemble of fits. All the uncertainties described previously are additive in nature and affect the significance of the branching fraction results. The total additive signal yield uncertainty is between 0.2 and 0.7 events, depending on the mode.

The sources of multiplicative uncertainties include: reconstruction efficiency from tracking (0.8% per track for the leptons and 0.7% for the kaon or pion, added linearly); neutral π^0 and K^0_S reconstruction efficiency (3.0% and 1.0%, respectively); charged particle identification (0.7% for electrons, 1.0% for muons, 0.2% for pions, 1.1% for kaons, added linearly); the BDT response from comparison to charmonium control samples such as $B^- \to J/\psi X^-$ (2.0%); and the number of $B\bar{B}$ pairs (0.6%) [12]. The total multiplicative branching fraction uncertainty is 5% or less for all modes.

When forming the overall branching fraction for the $B^+ \to K^{*-}\ell^+\ell'^+$ decays, we assume that the overall

K^{*-} submode additive uncertainties are uncorrelated and the multiplicative uncertainties are correlated.

As shown in Table I, we observe no significant yields. We use a Bayesian approach to calculate the 90% C.L. branching fraction upper limits $\mathcal{B}_{UL}$ by multiplying the likelihood distributions with a prior, which is null in the unphysical regions ($n_s < 0$) and constant elsewhere. The total likelihood distribution is integrated (taking into account statistical and systematic uncertainties) as a function of the branching fraction from 0 to $\mathcal{B}_{UL}$, such that $\int_0^{\mathcal{B}_{UL}} \mathcal{L}\, d\mathcal{B} = 0.9 \times \int_0^{\infty} \mathcal{L}\, d\mathcal{B}$. For the overall $K^{*-}\ell^+\ell'^+$ results, the total likelihood distributions for the two submodes are first combined before integration. The upper limits in all cases are dominated by the statistical uncertainty.

In summary, we have searched for eleven lepton-number violating processes $B^+ \to X^-\ell^+\ell'^+$. We find no significant yields and place 90% C.L. upper limits on the branching fractions in the range $(1.5\text{–}26) \times 10^{-7}$. The limits for the modes with a ρ^-, π^- or K^- are an order of magnitude more stringent than previous best measurements [10]. The limits for the $B^+ \to D^-\ell^+\ell'^+$ are compatible with those reported in Ref. [8].

We are grateful for the excellent luminosity and machine conditions provided by our PEP-II colleagues and for the substantial dedicated effort from the computing organizations that support *BABAR*. The collaborating institutions wish to thank SLAC for its support and kind hospitality. This work is supported by DOE and NSF (USA), NSERC (Canada), CEA and CNRS-IN2P3 (France), BMBF and DFG (Germany), INFN (Italy), FOM (Netherlands), NFR (Norway), MES (Russia), MICIIN (Spain), and STFC (United Kingdom). Individuals have received support from the Marie Curie EIF (European Union) and the A. P. Sloan Foundation (USA).

[1] F. R. Klinkhamer and N. S. Manton, Phys. Rev. D **30**, 2212 (1984).
[2] J. Beringer *et al.* (Particle Data Group), Phys. Rev. D **86**, 010001 (2012), section 13 and references therein.
[3] E. Majorana, Nuovo Cimento **14**, 171 (1937).
[4] A. Atre, T. Han, S. Pascali, and B. Zhang, J. High Energy Phys. 05 (**2009**) 030.
[5] S. Davidson, E. Nardi, and Y. Nir, Phys. Rep. **466**, 105 (2008).
[6] R. Aaij *et al.* (LHCb Collaboration), Phys. Rev. Lett. **108**, 101601 (2012); (LHCb Collaboration), Phys. Rev. D **85**, 112004 (2012).
[7] J. P. Lees *et al.* (*BABAR* Collaboration), Phys. Rev. D **85**, 071103 (2012).
[8] O. Seon *et al.* (Belle Collaboration), Phys. Rev. D **84**, 071106 (2011).
[9] Charge-conjugate modes are implied throughout this paper.
[10] K. W. Edwards *et al.* (CLEO Collaboration), Phys. Rev. D **65**, 111102 (2002).
[11] J. P. Lees *et al.* (*BABAR* Collaboration), Nucl. Instrum. Methods Phys. Res., Sect. A **726**, 203 (2013).
[12] B. Aubert *et al.* (*BABAR* Collaboration), Nucl. Instrum. Methods Phys. Res., Sect. A **479**, 1 (2002); B. Aubert *et al.* (*BABAR* Collaboration), *ibid.* **729**, 615 (2013).
[13] D. J. Lange, Nucl. Instrum. Methods Phys. Res., Sect. A **462**, 152 (2001).
[14] B. F. Ward, S. Jadach, and Z. Was, Nucl. Phys. B, Proc. Suppl. **116**, 73 (2003); T. Sjöstrand, Comput. Phys. Commun. **82**, 74 (1994).
[15] E. Barberio and Z. Was, Comput. Phys. Commun. **79**, 291 (1994).
[16] S. Agostinelli *et al.* (GEANT4 Collaboration), Nucl. Instrum. Methods Phys. Res., Sect. A. **506**, 250 (2003).
[17] G. C. Fox and S. Wolfram, Nucl. Phys. **B157**, 543 (1979).
[18] B. P. Roe, H.-J. Yang, J. Zhu, I. Stancu, and G. McGregor, Nucl. Instrum. Methods Phys. Res., Sect. A **543**, 577 (2005).
[19] S. Brandt, C. Peyrou, R. Sosnowski, and A. Wroblewski, Phys. Lett. **12**, 57 (1964); E. Farhi, Phys. Rev. Lett. **39**, 1587 (1977).
[20] B. Aubert *et al.* (*BABAR* Collaboration), Phys. Rev. Lett. **94**, 161803 (2005).
[21] R. Barlow, Nucl. Instrum. Methods Phys. Res., Sect. A **297**, 496 (1990).
[22] H. Albrecht *et al.* (ARGUS Collaboration), Z. Phys. C **48**, 543 (1990).
[23] The Cruijff function is a centered Gaussian with different left-right resolutions and non-Gaussian tails: $f(x) = \exp((x-m)^2/(2\alpha_{L,R}^2 + \alpha_{L,R}(x-m)^2))$.
[24] K. S. Cranmer, Comput. Phys. Commun. **136**, 198 (2001).
[25] T. Skwarnicki, Ph.D. thesis, Cracow Institute of Nuclear Physics, 1986 (unpublished).
[26] G. J. Gounaris and J. J. Sakurai, Phys. Rev. Lett. **21**, 244 (1968).
[27] W. Verkerke and D. P. Kirkby, The RooFit toolkit for data modeling, eConf C0303241, MOLT007 (2003).